HHS Public Access

Author manuscript

Pac Symp Biocomput. Author manuscript; available in PMC 2023 January 01.

Published in final edited form as:

Pac Symp Biocomput. 2022 ; 27: 121–132.

Effects of ApoE4 and ApoE2 genotypes on subcortical magnetic susceptibility and microstructure in 27,535 participants from the UK Biobank†

Talia M. Nir*, **Alyssa H. Zhu***, **Iyad Ba Gari**, **Daniel Dixon**, **Tasfiya Islam**, **Julio E. Villalon-Reina**

Imaging Genetics Center, Stevens Neuroimaging and Informatics Institute, Keck School of Medicine University of Southern California, Marina del Rey, California, 90292, USA

Sarah E. Medland

QIMR Berghofer Medical Research Institute, Brisbane, Australia

Paul M. Thompson, **Neda Jahanshad**

Imaging Genetics Center, Stevens Neuroimaging and Informatics Institute, Keck School of Medicine University of Southern California, Marina del Rey, California, 90292, USA

Abstract

Disrupted iron homeostasis is associated with several neurodegenerative diseases, including Alzheimer's disease (AD), and may be partially modulated by genetic risk factors. Here we evaluated whether subcortical iron deposition is associated with ApoE genotype, which substantially affects risk for late-onset AD. We evaluated differences in subcortical quantitative susceptibility mapping (QSM), a type of MRI sensitive to cerebral iron deposition, between either ApoE4 (E3E4+E4E4) or ApoE2 (E2E3+E2E2) carriers and E3 homozygotes (E3E3) in 27,535 participants from the UK Biobank (age: 45–82 years). We found that ApoE4 carriers had higher hippocampal (d=0.036; p=0.012) and amygdalar (d=0.035; p=0.013) magnetic susceptibility, particularly individuals aged 65 years or older, while those carrying ApoE2 (which protects against AD) had higher QSM only in the hippocampus (d=0.05; p=0.006), particularly those under age 65. Secondary diffusion MRI microstructural associations in these regions revealed greater diffusivity and less diffusion restriction in E4 carriers, however no differences were detected in E2 carriers. Disease risk conferred by ApoE4 may be linked with higher subcortical iron burden in conjunction with inflammation or neuronal loss in aging individuals, while ApoE2 associations may not necessarily reflect unhealthy iron deposits earlier in life.

Keywords

Quantitative Susceptibility Mapping; Diffusion MRI; Iron; APOE; Alzheimer's disease

†This work was completed using UK Biobank Resource under application number 11559.

TNir@usc.edu .

*These authors contributed equally to this work

1. Introduction

Iron is essential for normal brain function; however, disrupted iron homeostasis can lead to brain iron accumulation, which is associated with neurodegenerative diseases including Parkinson's and Alzheimer's disease (AD)[1]. Excess iron induces oxidative stress, and accompanies neuritic plaques and neurofibrillary tangles, the pathological hallmarks of AD[2]. Plasma levels of iron-regulating proteins, including ferritin and transferrin, are highly heritable, with a large portion of their heritability explained by variants in the *HFE* and *TF* genes[3]; variants in these genes have been associated specifically with iron overload[4]. Brain iron concentration and other microstructural properties may be detected *in vivo* using metrics derived from advanced MRI techniques, including susceptibility- and diffusion-weighted MRI sequences (SWI and dMRI, respectively). These metrics are also sensitive to genetic variants associated with iron homeostasis[5, 6].

Quantitative susceptibility mapping (QSM) derived from SWI is sensitive to paramagnetic iron concentrations, a predominant source of magnetic susceptibility variation in brain tissue. QSM has been used to study susceptibility profiles of iron-rich subcortical structures in both normal aging[7] and neurodegenerative diseases[8]. Tissue magnetic susceptibility is also influenced by factors such as calcium and myelin concentrations. While there is less myelin in subcortical gray matter structures than in white matter, myelin is diamagnetic and counteracts iron effects on QSM, thus confounding QSM interpretations.

Brain microstructure can also be evaluated with diffusion MRI (dMRI), which may help disentangle the opposing effects of iron and myelin on QSM. Single-shell diffusion tensor imaging (DTI) is the most widely used method to analyze dMRI datasets, but cannot differentiate crossing fibers, and captures partial volumes from different tissue compartments. This may reduce the sensitivity of DTI measures, in particular for evaluating complex gray matter micro-architecture. Multi-shell neurite orientation dispersion and density imaging (NODDI) is a three-compartment biophysical model that attempts to resolve signal contributions from various tissue compartments, including the restricted intracellular and 'freewater', or isotropic, extracellular compartments[9]. Such models may offer insight into subcortical microstructural properties and associations between QSM and genetic risk factors.

The most well-recognized, and greatest common genetic risk factor for sporadic AD is a haplotype in the *APOE* gene. ApoE plays a key role in cerebral cholesterol metabolism and β-amyloid clearance. Growing evidence suggests that AD risk conferred by the ApoE4 genotype (carried by around 25% of individuals, depending on ancestry) is partially linked with cerebral iron burden. For example, both higher magnetic susceptibility and its association with higher amyloid plaque load have been reported in ApoE4 carriers with mild cognitive impairment[10]. ApoE2, in contrast, has a proposed neurotrophic or neuroprotective effect[11]. However, as ApoE2 is less prevalent in the population (found in around 10% of people), few studies have been sufficiently well-powered to evaluate whether ApoE2 has an effect on brain structure or function[12]; none, to our knowledge, have investigated associations with QSM.

In this study, we evaluated associations between both ApoE4 and ApoE2 genotypes and *in vivo* QSM and dMRI measures of subcortical iron concentrations and microstructure in a large, population-based sample of older adults (age range: 45–82 years) from the UK Biobank[13].

2. Methods

2.1. UK Biobank Participants

The UK Biobank (UKBB) is a publicly available dataset of over 500,000 community-based middle-aged and older adults residing in the United Kingdom[13]. At the time of this analysis, nearly 43,000 of these individuals had undergone brain MRI on a 3T Siemens Skyra. SWI, dMRI, T2-weighted FLAIR, and T1-weighted (T1w) MRI were downloaded from the UKBB database through application 11559; available MRI acquisition protocols and preprocessing are detailed in Miller et al. (2016). In total, 40,069 participants had SWI and T1w images, 35,600 of whom also had dMRI. MRI scans that failed preprocessing or did not pass quality control (QC), as described for each modality below, were removed from analyses. Participants whose genetic ethnic group was not of European ancestry, who were missing demographic or genetic data, or whose available ApoE genotype was not E2E2, E2E3, E3E3, E3E4, or E4E4, were also excluded - leaving 27,535 participants with QSM and 27,313 participants with dMRI (Figure 1; Table 1).

2.2. T1-Weighted MRI

T1w 3D volumetric MPRAGE DICOMs were downloaded for processing ($1\times1\times1$ mm^3 voxels). FreeSurfer version 7.1 was used to obtain segmentations for seven subcortical regions of interest (ROIs): the thalamus, caudate, putamen, pallidum, hippocampus, amygdala, and nucleus accumbens. Participants with a subcortical volume laterality index ($LI=(L-R)/(L+R)$) greater than five standard deviations from the mean were flagged for visual inspection and possible removal from the analysis.

2.3. Quantitative Magnetic Susceptibility

QSM maps were derived from the SWI DICOMs ($0.8\times0.8\times3$ mm^3 voxels; TE=9.42, 20 ms) and constructed using the Morphology Enabled Dipole Inversion (MEDI) toolbox (http://pre.weill.cornell.edu/mri/pages/qsm.html). Magnitude images were isolated for each head coil channel (N=32) and then combined by taking the square root of the sum of squares. The resulting magnitude image was skull-stripped using HD-BET[14]. Phase images were combined across two echo times by using a complex fitting approach to estimate the frequency offset in each voxel[15]. The combined phase was unwrapped using the Laplacian operation method, and the background field was removed using the Laplacian Boundary Value[16]. Finally, the MEDI solver was implemented with model error reduction through iterative tuning (MERIT) and a spherical mean value (SMV) operator for background field removal (lambda=1000, SMV kernel=3)[15].

All QSM images were visually inspected for quality. Images were rated for overall image quality (pass/fail) and Gibbs ringing (on a scale of 0–2); images with poor image quality and severe Gibbs ringing (i.e., 2s) were removed. Each participant's SWI magnitude image

was linearly registered to their respective T1w image using FSL's *flirt* with 12 degrees-of-freedom (*dof*) and normalized mutual information; the resulting transform was then applied to the QSM image.

2.4. Diffusion-Weighted MRI

Multi-shell dMRI scans were preprocessed and available for download as previously described[17]. All dMRI were acquired with 2×2×2 mm^3 voxels and included 50 b=1000 s/mm^2 and 50 b=2000 s/mm^2 diffusion-weighted images (δ=21.4 ms, Δ=45.5 ms), and 5 b0 volumes. Two dMRI models were evaluated: 1) DTI, fit to the subset of b=0 and 1000 s/mm^2 volumes using FSL, was made available for download by the UKBB; 2) we further fit NODDI[9] to all shells using DmiPy[18]. Resulting DTI fractional anisotropy (FA) and mean diffusivity (MD) and NODDI intracellular (ICVF), isotropic volume fractions (ISOVF), and orientation dispersion index (ODI) maps were transformed to respective T1w images through a multi-step process.

The UKBB processing includes proprietary gradient distortion correction (GDC) of all modalities; UKBB processed dMRI, therefore, had to be warped to achieve correspondence with the non-GDC T1w and SWI images that we independently processed for this study. For each participant, the GDC mean b_0 image was linearly registered to the respective GDC T2-FLAIR, using FSL's *flirt* with 12 *dof* and a boundary-based registration (BBR) using the FreeSurfer-derived white matter mask, which in turn was non-linearly warped to the original T2-FLAIR using ANTs symmetric normalization. The T2-FLAIR was then linearly registered to the respective T1w image using FSL's *flirt* with 6 *dof* and BBR. The transformations from GDC b_0 to T1w were concatenated and applied to all dMRI scalar maps.

2.5. Statistical Analyses

The median QSM and diffusion values across voxels in each of the left and right subcortical ROIs were extracted. The average of the left and right medians was then calculated, and the bilateral averages used for analysis.

Multiple linear regressions were performed to evaluate differences in each of the seven regional QSM indices between ApoE3 homozygotes (E3E3) and either 1) ApoE4 carriers (E4E3 and E4E4) or 2) ApoE2 carriers (E2E3 and E2E2). Secondary analyses evaluated the additive effect of carrying one or two E4 or E2 alleles. Sixteen covariates were included in all statistical models: age, sex, age-by-sex interaction, age^2, age^2-by-sex interaction, educational attainment ("college" or "no college"), and population structure (measured using the first 10 principal components of the UKBB ancestry analysis). To correct for multiple comparisons across seven ROIs, we used the false discovery rate (FDR) procedure (q=0.05). All reported p-values are uncorrected; only associations for which p-values survived FDR correction were considered significant.

In regions that showed significant associations in primary analyses, we further evaluated 1) QSM effects beyond structural volume by also covarying for regional volume and total intracranial volume; and 2) associations between ApoE genotype and subcortical microstructure indexed with dMRI measures, using the same statistical models. We also

tested for ApoE-by-age interactions in these regions, as ApoE genotypes may have an age-dependent effect on the brain. Interaction analyses were conducted using both linear and generalized additive models (GAM), including ApoE genotype and age as covariates. The R `mgcv` package was used for GAM analyses; age, age-by-sex and ApoE-by-age interaction terms were modeled using spline smoothing functions (cubic regression splines, k = 10) in place of the linear and non-linear age-related covariate. Finally, we stratified linear associations by age, testing for ApoE associations within the subsets of participants either < 65 or ≥ 65 years of age.

3. Results

3.1. ApoE4 Microstructural Associations

Compared to the E3E3 group (N=16,590), E4 carriers (N=7,235 E3E4 and E4E4 combined) had higher magnetic susceptibility values in the hippocampus (d=0.036) and amygdala (d=0.035; $p \leq$ critical FDR p=0.013; Table 2; Figure 2). Using an additive model, E4 carriers only had significantly higher susceptibility values in the amygdala (r=0.018; $p \leq$ critical FDR p=0.005). Susceptibility effects remained when also covarying for regional volume (hippocampus d=0.030; p=0.036; amygdala d=0.036; p=0.010).

dMRI comparisons between the E3E3 group (N=16,473) and E4 carriers (N=7,116 E3E4 and E4E4 combined) revealed significantly higher hippocampal MD (d=0.069; $p=1.0\times10^{-6}$) and ISOVF (d=0.062; $p=1.2\times10^{-5}$) and lower FA (d=−0.044; p=0.002) and ICVF (d=−0.064; $p=6.7\times10^{-6}$) in E4 carriers; the E4 group also had higher MD (d=0.032; p=0.020) and ISOVF (d=0.037; p=0.009) in the amygdala. All dMRI associations remained significant when also covarying for volume.

3.2. ApoE2 Microstructural Associations

Compared to the E3E3 group (N=16,590), E2 carriers (N=3,710 E3E2 and E2E2 combined) had higher magnetic susceptibility values in the hippocampus using both the dominant (d=0.05; $p \leq$ critical FDR p=0.006) and additive approaches (r=0.02; $p \leq$ critical FDR p=0.005; Table 3). Susceptibility effects remained significant when covarying for volume (d=0.046; p=0.012).

No significant subcortical dMRI differences were found between the E3E3 group (N=16,473) and E2 carriers (N=3,674 E3E2 and E2E2).

3.3. ApoE-by-Age Interactions

No significant linear QSM ApoE4-by-age or ApoE2-by-age interactions were detected in the hippocampus or amygdala (Figure 3A, C). However, a significant ApoE4-by-age effect was found in the amygdala using GAM (estimated degrees of freedom = 5.64, F = 2.54, p = 0.016; Figure 3D).

For dMRI, a significant linear ApoE4-by-age interaction was detected in the hippocampus with ICVF (r=0.030; p=0.0009), ISOVF (r=0.029; $p=5.7\times10^{-5}$), and MD (r=0.033; $p=7.9\times10^{-5}$), and in the amygdala with ISOVF (r=0.018; p=0.016) and MD (r=0.016; p=0.010). E4 carriers showed greater increases in ISOVF and MD and decreases in ICVF

with increasing age (Figure 4). Using GAM, significant ApoE4-by-age interactions were also found in the hippocampus with ICVF (p=0.007), ISOVF (p=2.3×10^{-5}), and MD (p=2.7×10^{-5}), and in the amygdala with ISOVF (p=0.026) and MD (p=0.016). No ApoE2-by-age interactions were detected with linear or GAM models in relation to diffusion measures.

3.3.1. ApoE Associations Stratified by Age—When stratified by age, ApoE4 was significantly associated with QSM values in both the hippocampus and amygdala only in the subset of participants age 65 years and older (hippocampus d=0.049; p=0.015; amygdala d=0.062; p=0.002).

ApoE4 was also associated with diffusion measures in the hippocampus (ISOVF: d=0.093; p=5.6×10^{-6}; ICVF: d=−0.081; p=7.7×10^{-5}; MD: d=0.097; p=2.3×10^{-6}; FA: d=−0.056; p=0.007) and amygdala (ISOVF: d=0.050; p=0.016; MD: d=0.051; p=0.013) in the older subset, while no significant associations were detected in the younger group.

In contrast, E2 carriers younger than 65 years of age had, on average, higher hippocampal magnetic susceptibility (d=0.073; p=0.005) than those with the E3E3 genotype, but differences were not significant in the older subset.

As with the full sample, ApoE2 associations with hippocampal diffusion measures were not significant in either age group.

4. Discussion

With aging, iron dysregulation and accumulation can induce oxidative stress, trigger the aggregation of proteins involved in pathogenesis of neurodegenerative disorders, and cause cell death[2]. Here, we found higher QSM susceptibility in the hippocampi and amygdala of E4 carriers, temporal lobe structures known to be affected in AD and dementia; this likely reflects higher iron deposition, but may also be driven, in part, by less myelin. Several studies have found higher magnetic susceptibility in the hippocampi and amygdala of individuals with mild cognitive impairment and AD[8, 19]. To date, only a few studies have linked ApoE4 genotype with greater magnetic susceptibility and iron. Significantly higher cerebrospinal fluid ferritin levels have been found across cognitively normal and AD ApoE4 carriers (N=302)[20]. In a study by van Bergen et al. (2016), ApoE4 carriers had both higher cortical QSM iron deposition and cortical PiB-PET amyloid plaque load (N=37)[10]. Findings from yet another QSM study suggested that ApoE4 may moderate iron effects on default mode network connectivity in cognitively healthy older adults (N=69)[21]. Still, most published studies are relatively small and largely evaluate older individuals with cognitive impairment. Large-scale studies of the normal aging population are needed to better understand genetic risk for disease.

Higher QSM susceptibility in subcortical structures of E4 carriers was consistently accompanied by higher dMRI MD and ISOVF and lower FA and ICVF. These dMRI differences indicate greater diffusivity and less restriction, and could reflect, for example, lower neuronal density or greater inflammation and edema. Other studies have similarly reported lower FA and higher MD in white matter of older ApoE4 carriers[22]. Transgenic

mice expressing ApoE4 in neurons have been shown to develop axonal degeneration and gliosis in the brain[23]. Moreover, iron deposits are also found in activated microglia[24], the inflammatory cells of the nervous system, which, *post mortem*, have been found to colocalize with tau and amyloid in the hippocampi of individuals with AD[25].

Growing evidence suggests that ApoE4 effects on brain structure and function may become more pronounced after age 60; two relatively large studies suggest that ApoE4 does not affect cognitive function before age 65 (N=6,560)[26], and that in older individuals, ApoE4 carriers have a faster rate of cognitive decline than non-carriers (N=501)[27]. While smaller hippocampal volumes in ApoE4 carriers have been reported in young healthy carriers (N=44)[28], other studies have failed to find this association[29]. Smaller hippocampal and amygdalar volumes have more consistently been found in older ApoE4 carriers with cognitive impairment[29, 30]. Accordingly, in addition to significant ApoE4-by-age interactions indicating greater age-related increases in iron and diffusivity in E4 carriers, we found that QSM and dMRI E4 effects only survived in individuals over age 65.

ApoE2 has been associated with lower risk for AD[11]. While greater hippocampal volumes have been detected in E2 carriers in ADNI[30], to date, large scale population neuroimaging studies have found limited evidence to suggest it confers protection through improved brain integrity. Here, we found higher magnetic susceptibility in the hippocampi of E2 carriers in, to our knowledge, the first study to evaluate QSM differences. While this could reflect higher iron concentration, this does not necessarily reflect unhealthy deposits; it could, for example, be driven by hemoglobin in the surrounding vasculature and reflect greater blood circulation around the hippocampus. In contrast to ApoE4 carriers, who showed both higher QSM and compromised dMRI microstructural integrity, we did not detect any associations between the ApoE2 genotype and dMRI measures; this may suggest that subcortical iron depositions play a different role in E2 carriers. Furthermore, while no ApoE2-by-age interaction was found, ApoE2 effects were only detected in younger participants. This could reflect the important role iron plays in the central nervous system; cerebral iron increases quickly early in development and is necessary for myelin production, neurotransmitter synthesis and breakdown, and microglial activation, among other essential functions[2]. There is also evidence, however, that ApoE2 is not entirely benign, and is associated with an increased risk of cerebral amyloid angiopathy[11] and type 2 diabetes mellitus[31]. Further studies are necessary to disentangle the relationship between ApoE2 and cerebral iron.

As with all quantitative MRI methods, QSM values depend on acquisition and processing protocols[32, 33]. In the processing approach used here, we used the QSM values directly output from our pipeline without inter-individual harmonization through the use of a reference region. Ventricular CSF or specific white matter bundles may be used for this purpose, however choice of reference region is not standardized, and QSM variation within reference regions may further confound measurements[8]. It will be important to determine whether the choice of QSM processing affects the overall conclusions of this work.

As with DTI, since the inception of NODDI a number of limitations have also been identified. To avoid overparameterization, many model assumptions and fixed parameters are imposed that have not been widely validated and are highly dependent on acquisition

parameters[34]; this complicates the biological specificity and interpretability of resulting microstructural measures.

In the largest QSM study to evaluate ApoE genotypes to date, we found that higher subcortical iron burden is associated with ApoE4. Our findings also offer some initial insights into ApoE2 mechanisms. Both AD risk and protective genotypes showed higher magnetic susceptibility compared to the most common E3E3 genotype; however, these effects were driven by different age groups, and had inconsistent effects on diffusion metrics. Independent replication and further histopathological investigation of the effects of ApoE genotype on hippocampal iron deposition, and its relationship to age, is needed. QSM provides complementary information to more commonly acquired MRI modalities, and acquisition of these scans in prospective studies of aging may provide further insights into neurodegeneration.

Acknowledgments

This work is supported in part by NIH grants: R01 AG059874, T32 AG058507, P41 EB015922, a Zenith Award from the U.S. Alzheimer's Association, and an image processing grant from Biogen Inc.

References

1. Raven EP, et al. , Increased iron levels and decreased tissue integrity in hippocampus of Alzheimer's disease detected in vivo with magnetic resonance imaging. J Alzheimers Dis, 2013. 37(1): 127–36. [PubMed: 23792695]
2. Ward RJ, et al. , The role of iron in brain ageing and neurodegenerative disorders. The Lancet. Neurology, 2014. 13(10): 1045–1060. [PubMed: 25231526]
3. Benyamin B, et al. , Variants in TF and HFE explain approximately 40% of genetic variation in serum-transferrin levels. Am J Hum Genet, 2009. 84(1): 60–65. [PubMed: 19084217]
4. Bell S, et al. , A genome-wide meta-analysis yields 46 new loci associating with biomarkers of iron homeostasis. Communications Biology, 2021. 4(1): 156. [PubMed: 33536631]
5. Elliott LT, et al. , Genome-wide association studies of brain imaging phenotypes in UK Biobank. Nature, 2018. 562(7726): 210–216. [PubMed: 30305740]
6. Jahanshad N, et al. , Brain structure in healthy adults is related to serum transferrin and the H63D polymorphism in the HFE gene. Proc Natl Acad Sci, 2012. 2012: 201105543.
7. Zhang Y, et al. , Longitudinal data for magnetic susceptibility of normative human brain development and aging over the lifespan. Data in Brief, 2018. 20: 623–631. [PubMed: 30197920]
8. Ravanfar P, et al. , Systematic Review: Quantitative Susceptibility Mapping (QSM) of Brain Iron Profile in Neurodegenerative Diseases. Frontiers in Neuroscience, 2021. 15(41).
9. Zhang H, et al. , NODDI: practical in vivo neurite orientation dispersion and density imaging of the human brain. Neuroimage, 2012. 61(4): 1000–16. [PubMed: 22484410]
10. van Bergen JMG, et al. , Colocalization of cerebral iron with Amyloid beta in Mild Cognitive Impairment. Scientific Reports, 2016. 6: 35514–35514. [PubMed: 27748454]
11. Li Z, et al. , APOE2: protective mechanism and therapeutic implications for Alzheimer's disease. Molecular Neurodegeneration, 2020. 15(1): 63. [PubMed: 33148290]
12. Grothe MJ, et al. , Multimodal characterization of older APOE2 carriers reveals selective reduction of amyloid load. Neurology, 2017. 88(6): 569–576. [PubMed: 28062720]
13. Miller KL, et al. , Multimodal population brain imaging in the UK Biobank prospective epidemiological study. Nature Neuroscience, 2016. 19(11): 1523–1536. [PubMed: 27643430]
14. Isensee F, et al. , Automated brain extraction of multisequence MRI using artificial neural networks. Human Brain Mapping, 2019. 40(17): 4952–4964. [PubMed: 31403237]

15. Liu T, et al. , Nonlinear formulation of the magnetic field to source relationship for robust quantitative susceptibility mapping. Magn Reson Med, 2013. 69(2): 467–76. [PubMed: 22488774]
16. Zhou D, et al. , Background field removal by solving the Laplacian boundary value problem. NMR in Biomedicine, 2014. 27(3): 312–319. [PubMed: 24395595]
17. Alfaro-Almagro F, et al. , Image processing and Quality Control for the first 10,000 brain imaging datasets from UK Biobank. NeuroImage, 2018. 166: 400–424. [PubMed: 29079522]
18. Fick RHJ, et al. , The Dmipy Toolbox: Diffusion MRI Multi-Compartment Modeling and Microstructure Recovery Made Easy. Frontiers in Neuroinformatics, 2019. 13(64).
19. Acosta-Cabronero J, et al. , In vivo quantitative susceptibility mapping (QSM) in Alzheimer's disease. PLoS One, 2013. 8(11): e81093. [PubMed: 24278382]
20. Ayton S, et al. , Ferritin levels in the cerebrospinal fluid predict Alzheimer's disease outcomes and are regulated by APOE. Nature Communications, 2015. 6(1): 6760.
21. Kagerer SM, et al. , APOE4 moderates effects of cortical iron on synchronized default mode network activity in cognitively healthy old-aged adults. Alzheimers Dement (Amst), 2020. 12(1): e12002. [PubMed: 32211498]
22. Harrison JR, et al. , Imaging Alzheimer's genetic risk using diffusion MRI: A systematic review. NeuroImage: Clinical, 2020. 27: 102359. [PubMed: 32758801]
23. Tesseur I, et al. , Prominent Axonopathy and Disruption of Axonal Transport in Transgenic Mice Expressing Human Apolipoprotein E4 in Neurons of Brain and Spinal Cord. The American Journal of Pathology, 2000. 157(5): 1495–1510. [PubMed: 11073810]
24. Connor JR, et al. , A histochemical study of iron, transferrin, and ferritin in Alzheimer's diseased brains. Journal of Neuroscience Research, 1992. 31(1): 75–83. [PubMed: 1613823]
25. Zeineh MM, et al. , Activated iron-containing microglia in the human hippocampus identified by magnetic resonance imaging in Alzheimer disease. Neurobiol Aging, 2015. 36(9): 2483–500. [PubMed: 26190634]
26. Jorm AF, et al. , APOE genotype and cognitive functioning in a large age-stratified population sample. Neuropsychology, 2007. 21(1): 1–8. [PubMed: 17201525]
27. Schiepers OJ, et al. , APOE E4 status predicts age-related cognitive decline in the ninth decade: longitudinal follow-up of the Lothian Birth Cohort 1921. Mol Psychiatry, 2012. 17(3): 315–24. [PubMed: 21263443]
28. O'Dwyer L, et al. , Reduced hippocampal volume in healthy young ApoE4 carriers: an MRI study. PloS One, 2012. 7(11): e48895–e48895. [PubMed: 23152815]
29. Lupton MK, et al. , The effect of increased genetic risk for Alzheimer's disease on hippocampal and amygdala volume. Neurobiology of aging, 2016. 40: 68–77. [PubMed: 26973105]
30. Hostage CA, et al. , Dissecting the gene dose-effects of the APOE ε4 and ε2 alleles on hippocampal volumes in aging and Alzheimer's disease. PLoS One, 2013. 8(2): e54483. [PubMed: 23405083]
31. Santos-Ferreira C, et al. , Apolipoprotein E2 Genotype Is Associated with a 2-Fold Increase in the Incidence of Type 2 Diabetes Mellitus: Results from a Long-Term Observational Study. Journal of Lipids, 2019. 2019: 1698610. [PubMed: 31485353]
32. Deistung A, et al. , Overview of quantitative susceptibility mapping. NMR in Biomedicine, 2017. 30(4): e3569.
33. Haacke EM, et al. , Quantitative susceptibility mapping: current status and future directions. Magnetic Resonance Imaging, 2015. 33(1): 1–25. [PubMed: 25267705]
34. Jelescu IO and Budde MD, Design and Validation of Diffusion MRI Models of White Matter. Frontiers in Physics, 2017. 5(61).

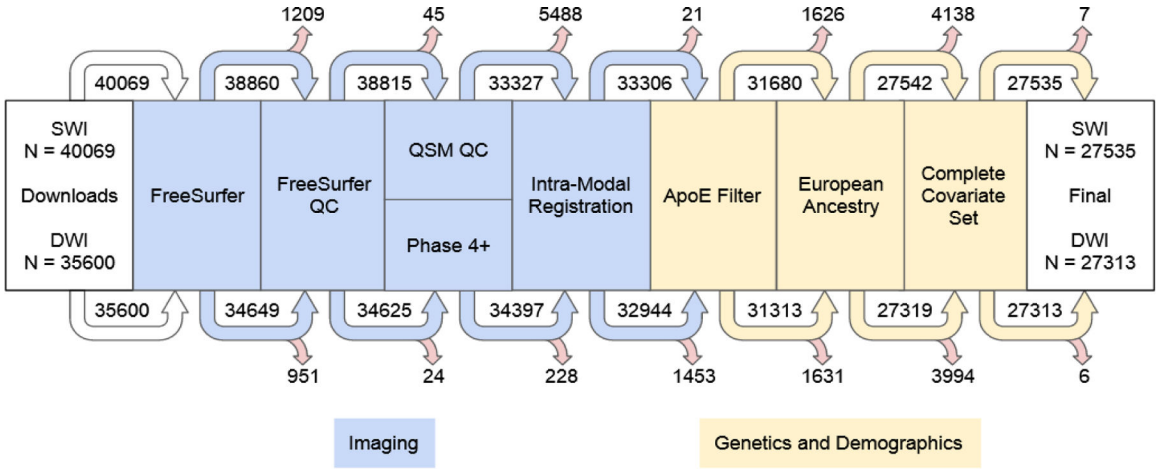

Figure 1.
Processing stream with remaining number of participants after each step.

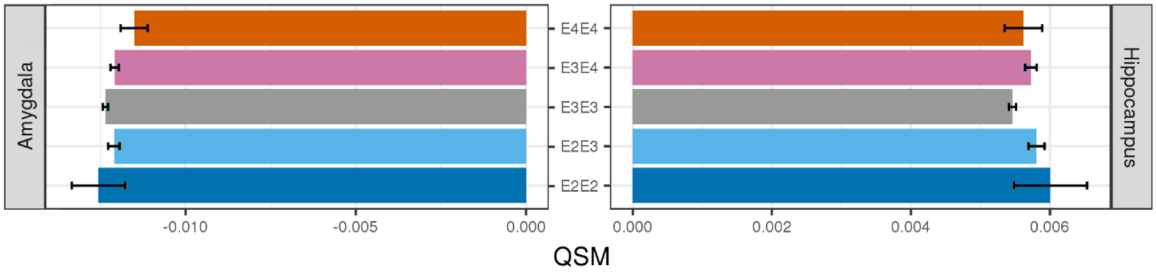

Figure 2.
Bar plots of QSM values in the hippocampus and amygdala by ApoE genotype.

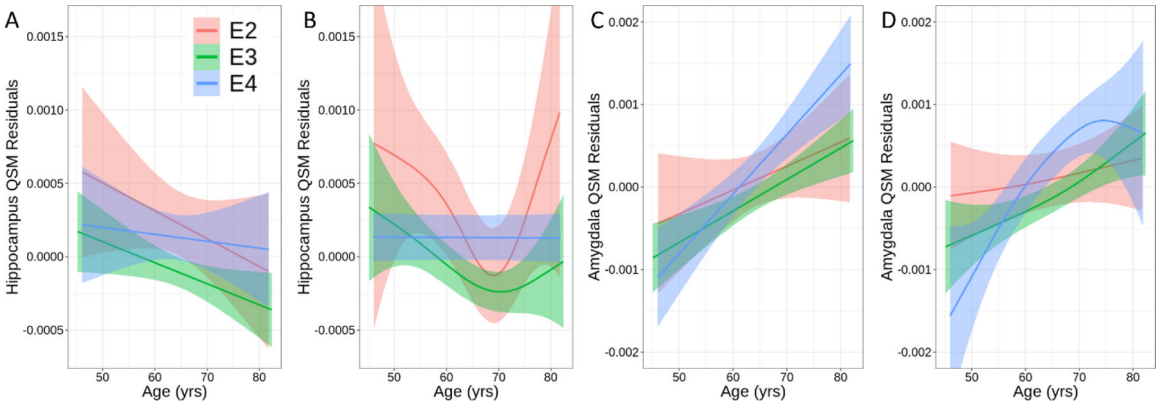

Figure 3.

QSM residuals in the **(A, B)** hippocampus and **(C, D)** amygdala plotted against age using either **(A, C)** a linear approach (adjusted for sex, age-by-sex, age^2, education, and population structure), or **(B, D)** using GAM (linearly adjusted for sex, age-by-sex, age^2-by-sex, education, and population structure).

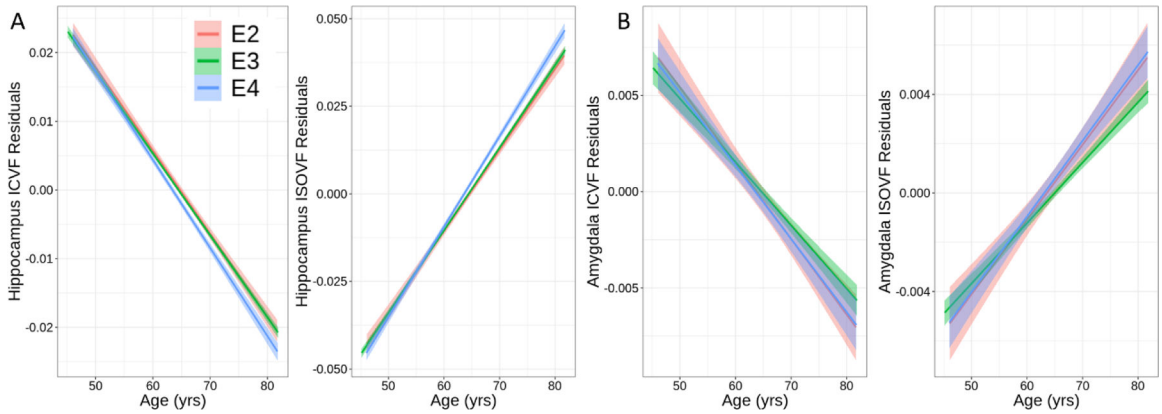

Figure 4.

ICVF and ISOVF dMRI residuals (adjusted for sex, age-by-sex, age^2, education, and population structure) in the **(A)** hippocampus and **(B)** amygdala linearly plotted against age. MD plots closely resembled ISOVF, and GAM plots closely resembled linear plots.

Table 1.

ApoE genotype and demographic data for UKBB participants with QSM and dMRI.

ApoE	QSM						dMRI					
	Total N (%)	**Sex, Male N**	**Age yrs Mean (SD)**	**< 65, yrs N**	**≥ 65, yrs N**	**Edu, College N**	**Total N (%)**	**Sex, Male N**	**Age yrs Mean (SD)**	**< 65, yrs N**	**≥ 65, yrs N**	**Edu, College N**
E3E3	16,590 (60.3)	7,687	64.6 (7.6)	8,095	8,495	11,164	16,473 (60.3)	7,878	64.3 (7.5)	8,236	8,237	11,090
E3E4	6,589 (23.9)	2,996	64.1 (7.6)	3,440	3,149	4,508	6,522 (23.9)	3,006	63.8 (7.4)	3,461	3,061	4,417
E4E4	646 (2.3)	285	63.7 (7.1)	352	294	451	644 (2.4)	291	63.7 (7.1)	349	295	461
E2E3	3,538 (12.8)	1,586	64.9 (7.6)	1,690	1,848	2,369	3,510 (12.9)	1,656	64.5 (7.5)	1,725	1,785	2,346
E2E2	172 (0.6)	77	64.1 (8.2)	88	84	121	164 (0.6)	77	64.0 (8.0)	87	77	109
Total	27,535	12,631	64.5 (7.6)	13,665	13,870	18,613	27,313	12,908	64.2 (7.4)	13,858	13,455	18,423

Table 2.

ApoE4 associations with QSM.

ROI	Dominant					Additive			
	d	***r***	***b***	***se***	***p***	***r***	***b***	***se***	***p***
Thalamus	−0.002	0.001	-7.8×10^{-6}	4.6×10^{-5}	0.87	0.004	-2.5×10^{-5}	4.1×10^{-5}	0.54
Caudate	−0.020	0.009	-2.2×10^{-4}	1.5×10^{-4}	0.15	0.013	-2.8×10^{-4}	1.3×10^{-4}	0.040 *
Putamen	0.009	0.004	1.2×10^{-4}	1.8×10^{-4}	0.50	0.003	7.4×10^{-5}	1.6×10^{-4}	0.63
Pallidum	−0.018	0.008	-2.9×10^{-4}	2.3×10^{-4}	0.21	0.011	-3.4×10^{-4}	2.0×10^{-4}	0.090
Hippocampus	**0.036**	**0.016**	$\mathbf{2.4\times10^{-4}}$	$\mathbf{9.3\times10^{-5}}$	**0.012** **	0.015	1.9×10^{-4}	8.2×10^{-5}	0.022 *
Amygdala	**0.035**	**0.016**	$\mathbf{3.5\times10^{-4}}$	$\mathbf{1.4\times10^{-4}}$	**0.013** **	**0.018**	$\mathbf{3.5\times10^{-4}}$	$\mathbf{1.2\times10^{-4}}$	**0.005** **
Accumbens	−0.003	0.001	-5.5×10^{-5}	2.8×10^{-4}	0.85	0.004	-1.6×10^{-4}	2.5×10^{-4}	0.52

** uncorrected $p \leq$ critical FDR threshold

* uncorrected $p \leq 0.05$

Table 3.

ApoE2 associations with QSM.

ROI	Dominant					Additive			
	d	***r***	***b***	***se***	***p***	***r***	***b***	***se***	***p***
Thalamus	0.004	0.002	1.3×10^{-5}	5.9×10^{-5}	0.83	2.1×10^{-5}	-1.7×10^{-7}	5.6×10^{-5}	1.00
Caudate	0.024	0.009	2.6×10^{-4}	2.0×10^{-4}	0.18	5.4×10^{-3}	1.4×10^{-4}	1.8×10^{-4}	0.45
Putamen	0.014	0.005	1.7×10^{-4}	2.3×10^{-4}	0.46	2.4×10^{-3}	7.3×10^{-5}	2.1×10^{-4}	0.73
Pallidum	0.002	0.001	3.5×10^{-5}	2.9×10^{-4}	0.91	2.9×10^{-3}	-1.1×10^{-4}	2.7×10^{-4}	0.68
Hippocampus	**0.050**	0.019	$\mathbf{3.3\times10^{-4}}$	$\mathbf{1.2\times10^{-4}}$	0.006 **	$\mathbf{2.0\times10^{-2}}$	$\mathbf{3.1\times10^{-4}}$	$\mathbf{1.1\times10^{-4}}$	**0.005** **
Amygdala	0.021	0.008	2.1×10^{-4}	1.8×10^{-4}	0.24	7.2×10^{-3}	1.7×10^{-4}	1.7×10^{-4}	0.30
Accumbens	0.022	0.008	4.4×10^{-4}	3.7×10^{-4}	0.23	8.2×10^{-3}	4.0×10^{-4}	3.4×10^{-4}	0.24

** uncorrected $p \leq$ critical FDR threshold

* uncorrected $p \leq 0.05$